Science of Sintering, **53** (2021) 91-117

https://doi.org/10.2298/SOS2101091S

UDK: 628.3.03.034.2; 551.463.5; 551.524.2

Adsorption of Anthraquinone Dye AB111 from Aqueous Solution using Synthesized Alumina-Iron Oxide Doped Particles

Stevan S. Stupar[1*)], Marija M. Vuksanović[2], Ljubica M. Totovski[3], Radmila M. Jančić Heinemann[1], Dušan Ž. Mijin[1]

[1]University of Belgrade, Faculty of Technology and Metallurgy, Karnegijeva 4, 11120 Belgrade, Serbia

[2]University of Belgrade, Department of Chemical Dynamics and Permanent Education, „VINČA" Institute of Nuclear Sciences - National Institute of the Republic of Serbia, Mike Petrovića Alasa 12-14, 11351 Belgrade, Serbia

[3]Ministry of Defence, Military Technical Institute, Ratka Resanovica 1, 11030 Belgrade, Serbia

Abstract:

Adsorption of anthraquinone dye Acid Blue 111 by alumina-iron oxide doped particles prepared by sol-gel method from aqueous solutions was studied. The adsorbent morphology was revealed by FESEM and the crystallographic phase is analyzed by the XRD technique. The effect of adsorbate and adsorbent concentrations, pH value, type of adsorbent and thermodynamic parameters on dye removal by adsorption was studied. The change of dye concentration during the adsorbtion was followed using the UV-Visible spectrophotometer. The change of the adsorbent surface before and after dye removal was observed using the Fourier Transformation-infrared spectroscopy (FT-IR). The adsorption kinetics is in accordance with the pseudo-second-order kinetics model. The Langmuir and Freundlich adsorption isotherm models were used to describe the adsorption process. The thermodynamic study of dye adsorption proves the process is spontaneous with exothermic nature.

Keywords*: Textile industry wastewater; Alumina-iron oxide doped particles; Dye removal; Adsorbent characterization; Kinetics study.*

1. Introduction

With the rapid development of civilization, more demanding requirements in water quality have been set in the industry as well. Replacement of natural dyes with synthetic dyes in the processes of the textile industry gives positive characteristics as greater resistance to environmental influences, low production cost, a wider range of dyes and easy application on different materials [1]. Beside mentioned positive characteristics, synthetic dyes are highly toxic, non-biodegradable, mutagenic and carcinogenic substances witch presence in influent water can inhibit processes in their ecosystems [2-4]. Anthraquinone dyes are the second most used colorants with 15 % of all produced dyes and mostly used in the textile industry [5]. C. I. Acid Blue 111 (CAS 6420-90-4, C.I.62155, Fig. 1) is one of the colorants with anthraquinone chromophore in the structure.

*) **Corresponding author:** stevan.stupar13@gmail.com

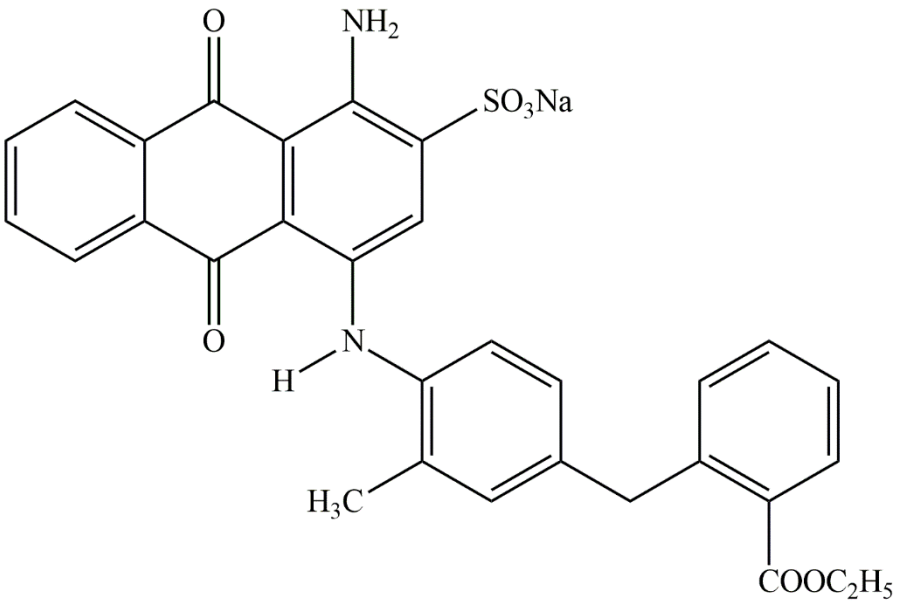

Fig. 1. The structure of AB111.

Undoubtedly, due to the high toxicity and the ability to inhibit biological process which is conventional wastewater treatment, in recent years the research are directed to environmental-friendly removal methods for dye elimination from waste waters before releasing into the recipient as adsorption [6], electrochemical oxidation [7], and different advanced oxidation processes [8], etc.

Adsorption represents the mass transfer process between solid substances-adsorbent, which has characteristic to remove dissolved pollutant particles from wastewater by selective attracting of the pollutants on the adsorbent surface. Depending on the bonding between the adsorbent surface and molecules of pollutants, adsorption can be classified as chemical or physical. Dye adsorption is usually a physical method which is based on Vander Waals forces and dipole-dipole interactions etc. Characteristics that also affect the adsorption are the polarity of adsorbent surface, particle size, particle polarity and size, etc. [9].

Alumina is a low-cost material and has a wide range of usage. Depending on the preparation method, this material can have adsorbent [10], direct current (DC) volume resistivity [11], antibacterial [12], good mechanical properties [13-14], etc. properties. The important advantage, besides the low-cost production, of alumina and alumina-based particles as adsorbent of pollutants from aqueous solutions is an eco-frendly and easy removal meterial [9, 15]. The previous examination of textile dye adsorptive decolourization, shows good adsorption characteristics for removal of azo dyes Reactive Orange 16 [16], Cibacron reactive yellow [17], anthraquinone dye Alizarin red S [18]. According to our knowledge, the adsorption of textile dye AB111 has not been examined using any adsorbent materials.

Alumina has one stable crystallographic phase that is known as corundum. This phase is obtained in various natural occurring crystals and is known for high strengths and hardness. On the other hand, when alumina is prepared by the sol-gel technique the precursors are soluble compounds of aluminium and trough the series of hydroxide and oxide forms the structure can be optimized for the adsorption [16, 19] or another use. It is known that the metastable forms of alumina such as γ-alumina are used for their high adsorption capacity and the openness of their structure that enables the creation of particles having a high surface to mass ratios. Other forms of alumina such as κ and η could be potentially good for the removal of organic matter from solutions. Those structures are usually analyzed by X-ray diffraction (XRD) technique and the crystallographic structure as well as the size of crystallites can be

obtained this way. The morphological structure of the adsorbent is revealed by SEM imaging techniques and the size and form of the used adsorbent can be described using some shape factors. The characteristics of the surface, eventual presence of OH groups or other adsorbed materials can be identified using the FT-IR technique [20].

In our study of Fenton and electro Fenton reactions [21], an attempt was made to prepare a ferrous bearing catalyst. It turned out that the obtained materials are better adsorbents than catalysts. So in this study, we report an investigation of the adsorption capacity of alumina-iron oxide doped particles prepared by sol-gel method with different content of iron at different temperatures. The influence of different initial parameters such as dye and alumina particles concentration, pH and temperature, was studied. The Langmuir and Freundlich adsorption isotherm models and thermodynamic parameters were used to describe the adsorption process. Dye removal during the time using alumina-iron oxide doped particles as adsorbent was followed by ultraviolet-visible (UV/Vis) spectroscopy.

2. Experimental Procedures

2.1. Materials and characterization methods

The alumina-iron oxide doped particles were prepared from aluminum hydroxide chloride (Locron L; $Al_2(OH)_5Cl{\cdot}2.5\ H_2O$) purchased from Clariant. The particles precursors were doped with $FeCl_3{\cdot}6H_2O$ purchased from Sigma-Aldrich.

The alumina-iron oxide doped particles were used as adsorbent of anthraquinone dye Acid Blue 111 produced by Hoechst A. G., Germany from aqueous solution. The crystallographic phases of sintered particles were determined by X-ray diffraction. The XRD sample was taken with Ital Structure APD2000 X-ray diffractometer in Bragg-Brentano geometry using CuKα radiation (λ = 1.5418 A) and scan mode (range: 20-75° 2θ, step: 0.50 s, step width: 0.02°).

Fourier-transfer infrared spectroscopy was used for structural analysis of particles. The analogs were fixed on a Nicolet 6700 spectrometer (Thermo Scientific) in attenuated total reflectance (ATR) mode using a one-way 45° F ATR accessory with diamond crystal and electronically cooled DTGS detector. The spectra were co-added to 64 scans at a spectral resolution of 4 cm^{-1} and corrected for ATR. The Nicolet 6700 FT-IR spectrometer was equipped with OMNIC software and recorded spectra in the wavelength range 2.5 to 20 μm (i.e. 4000 cm^{-1} to 500 cm^{-1}).

The morphologies of the alumina-iron oxide doped particles were examined using a field emission scanning electron microscope (FESEM), MIRA3 TESCAN, operated at 20 kV.

The adsorption method used comprised usage of the anthraquinone dye solution, Acid Blue 111 (Hoechst A. G., Germany) and the synthesized different alumina-iron oxide doped particles of known concentration in a thermostated glass reactor. Adjustment of the pH value of the solution was performed using 0.1 M sulfuric acid (Sigma-Aldrich (USA)). All the necessary chemicals used in the study were of analytical grade and used without further purification. Deionized water obtained from the Millipore Waters Milli-Q (USA) purification system was used.

The changes in dye concentrations in the liquid phase were followed using a UV-Vis spectrophotometry (UV-Vis Shimadzu 1800 spectrophotometer, Japan). The pH measurements were performed using a Hanna pH Meter HI-2210 (Italy). The magnetic stirrer was produced by Heidolph (Germany). All samples after adsorption are centrifuged on centrifuge Mini Spin® (Eppendorf). The influence of temperature on adsorption efficiency was tested by adjusting the temperature in a Maple scientific circulating water bath SB-5 (United Kingdom).

2.2. Synthesis of doped alumina particles

The synthesis of alumina-iron oxide doped particles using the sol-gel techniquehas been described in previous papers [22-24]. The alumina-iron oxide doped particles were synthesized by the sol-gel technique with the addition of different concentration of $FeCl_3 \cdot 6H_2O$ varying the temperature of calcination. Aluminium hydroxide chloride and $FeCl_3 \cdot 6H_2O$ were dissolved in water on a magnetic stirrer and then poured into a petri dish to dry. The gel was milled in a laboratory mortar and then the powder was calcinated at three different temperatures: 700, 800 and 900 °C for 2 h, to obtain different crystalline structures. Alumina particles doped with Fe_2O_3 were prepared with the addition of 4 wt.% and 13 wt.% of $FeCl_3 \cdot 6H_2O$. The alumina particles with 13 wt.% of $FeCl_3 \cdot 6H_2O$ were calcinated only at 800 °C.

All adsorption experiments were examined in a glass reactor containing 100 cm^3 of dye solution and initial concentration of the adsorbent. The reaction solution was mixed by a magnetic stirrer at a rate of 750 rpm. Kinetics analysis was performed at room temperature (298 K) and investigation of temperature influence on dye adsorption was examined at 298, 303, 308 and 318 K. All temperature adjustments were performed in a thermostatic bath. The solid adsorbent was separated after 60 minutes of adsorption processes by 120 seconds long centrifugation at 13500 rpm. The concentration of AB111 dye in these solutions was measured using UV-Vis spectroscopy at a wavelength of 634 nm.

The adsorption of AB111 can be described best by the pseudo-second-order kinetics model. Adsorption capacity q_t ($mg_{AB111}/g_{alumina}$) was calculated by using Equation 1 [1]:

$$q_t = \frac{(C_0 - C_t)V}{W} \qquad (1)$$

where C_0 (mg/L) and Ct (mg/L) were the concentrations of AB111 dye at t=0 (initial) and at time t (min), V (L) was the volume of the sample solution and W (g) was the weight of the adsorbent.

In this study, the efficiency of anthraquinone dye adsorption is represented by the percentage of dye removal. The percentage of dye removal was calculated by using Equation 2 [5]:

$$\%\ of\ dye\ removal = \frac{C_0 - C_t}{C_0} x100 \qquad (2)$$

where C_0 and C_t were described in explanation of Equation 1.

All the experiments were carried out under controlled conditions: the temperature in the thermostatic bath was maintained constant to within ± 0.1°C, the adsorbent samples were weighed to four-digit accuracy, and the solution concentrations were determined with four-digit accuracy. At least three measurements were done for each determination.

3. Results and Discussion

3.1. Characterization of alumina-iron oxide doped particles

The morphology of alumina-iron oxide doped particles was studied by SEM analysis. The SEM photographs obtained from Scanning Electron Microscopy analysis are presented in Figs. 2-4 shows the SEM photographs, Energy-dispersive X-ray spectroscopy and distribution of diameter of the alumina-iron oxide doped particles sintered at 800 °C with 4 wt.% (Fig. 3) and 13 (Fig. 4) wt.% of $FeCl_3 \cdot 6H_2O$.

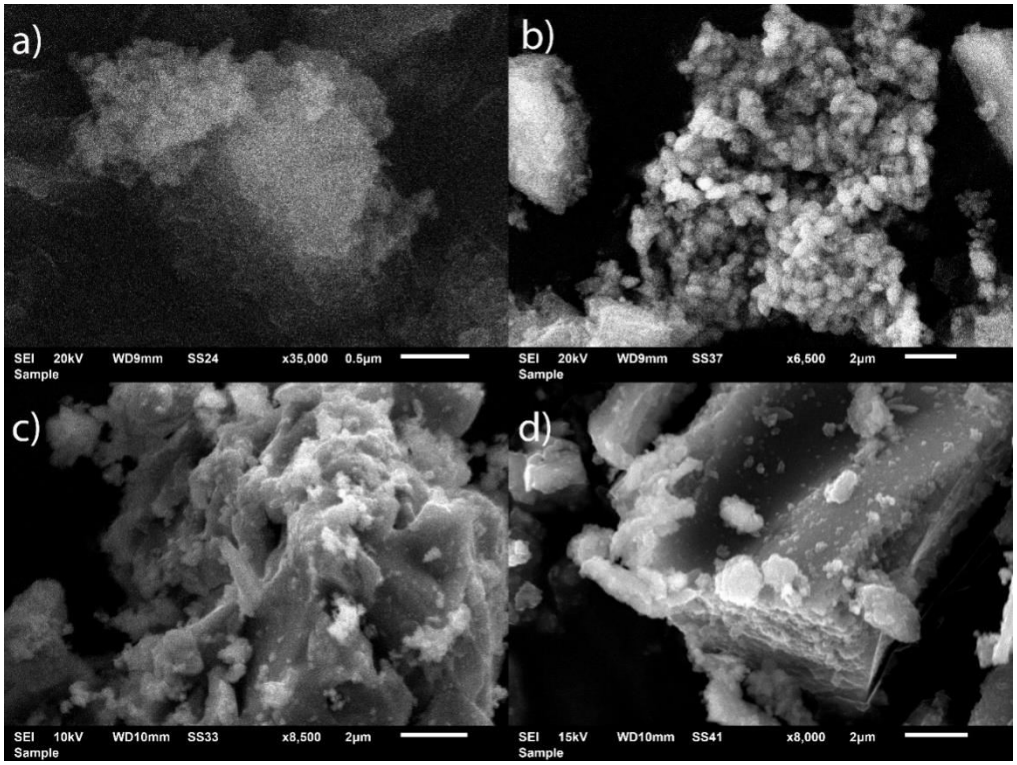

Fig. 2. The SEM photographs of alumina-iron oxide doped particles sintered at (a) 700 ℃ – 4 wt% Fe, (b) 800 ℃ – 4 wt.% Fe, (c) 900 °C – 4 wt.% Fe and (d) 800 °C – 13 wt% Fe.

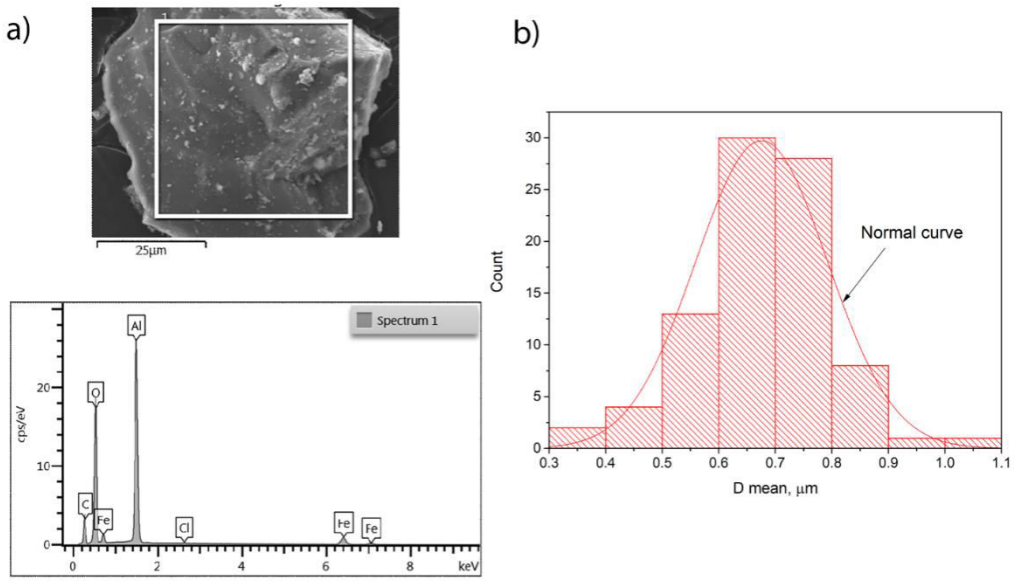

Fig. 3. a) SEM photograph and Energy-dispersive X-ray spectroscopy of alumina-iron oxide doped particles sintered at 800 °C with the addition of 4 wt.% of $FeCl_3 \cdot 6H_2O$ and b) distribution of diameter of the particles.

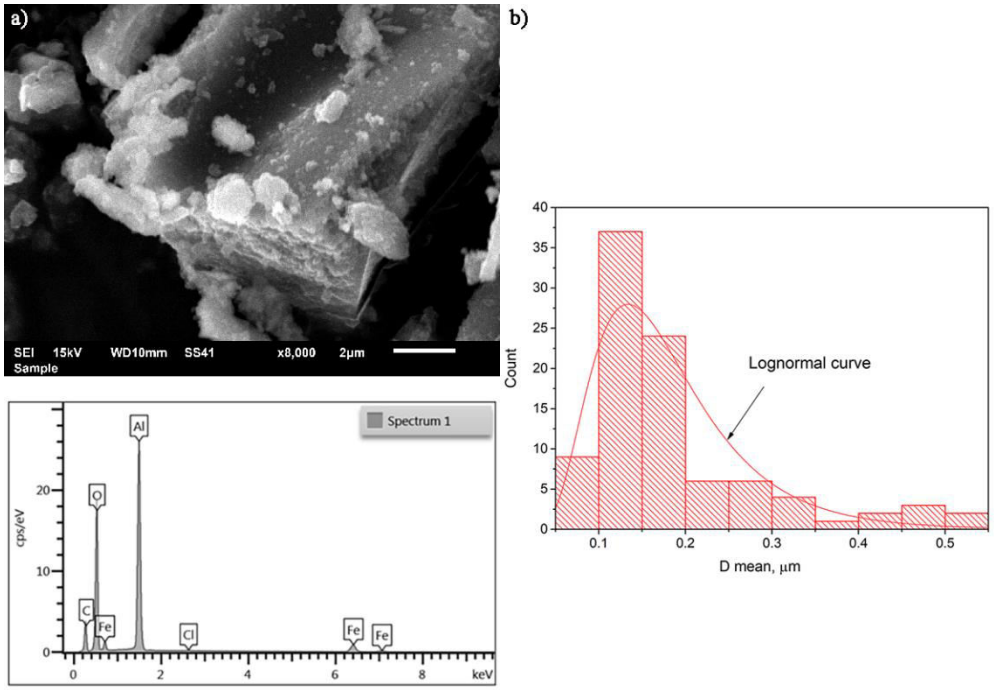

Fig. 4. a) SEM photograph and Energy-dispersive X-ray spectroscopy of alumina-iron oxide doped particles sintered at 800 °C with the addition of 13 wt.% of $FeCl_3 \cdot 6H_2O$ and b) distribution of diameter of the particles.

Energy-dispersive X-ray spectroscopy of the marked area of SEM photograph shows the weight percent (wt.%) of different mass fraction of alumina-iron oxide doped particles. In alumina-iron oxide doped partices with addition of 4 wt.% of $FeCl_3 \cdot 6H_2O$ the presence of aluminium, oxygen, iron and chlorine were 56.52, 37.90, 4.63 and 0.95 wt.%, respectively. In η–Al_2O_3 800 °C-13 wt.% Fe presence of same elements are presented in Fig. 4 were 46.07, 44.12, 9.44, 0.23 wt.%, respectively. The presence of chlorine is caused by impurities remaining after the synthesis process, originates from precursors, $Al_2(OH)_5Cl \cdot 2.5\ H_2O$ and $FeCl_3 \cdot 6H_2O$. Other elements represent the desired chemical composition of the synthesized powder. From the EDS data the exact weight percent of Fe_2O_3 in the first specimen was 4.01 wt.% and in the second specimen it was 13.05 wt.%. Those compositions are in accordance with the XRD data where in the first specimen the presence of the hematite is less visible as the alumina structures dominante the crystal structure. The corresponding mol fractions of Fe_2O_3 in the two particle systems are 3.69 wt.% of Fe_2O_3 and 8.7 wt.% of Fe_2O_3. Comparing to the calculated phase diagram of Al_2O_3-Fe_2O_3 system those two compositions correspond to two different situations of oxide solubilites. The concentration of 3.69 mol.% correspond to the structure where the hematite is dissolved in alumina and thus the dominate structure is alumina and the presence of the hematite is less visible. The role of the present hematite is mostly to ease the formation of corundum structure in the system. On the other hand superior concentrations of Fe_2O_3 correspond to the two phase area in the phase diagram where the hematite and alumina are present separately and this is visible from the XRD. In the specimen having 8.7 wt.% of the Fe_2O_3 the presence of the hematite structure is obvious [25].

The distribution of particle size was done using the images where individual particles were distinguishable and their diameters were measured using the image analysis software. The large particles visible in SEM images are mostly agglomerates and they are mostly dispersed in the process. According to Figs 3 and 4, the alumina-iron oxide doped particles sintered at the same temperature with 4 wt.% of $FeCl_3 \cdot 6H_2O$ is mostly in the range 0.5-0.7

μm. Unlike the previous specimen, alumina-iron oxide doped particles with 13 wt.% of $FeCl_3 \cdot 6H_2O$ is mostly in the range 0.1-0.2 μm.

The values of point of zero charge for alumina-iron oxide doped particles with 4 wt.% of $FeCl_3 \cdot 6H_2O$ sintered at 700, 800, and 900 °C and alumina-iron oxide doped particles with 13 wt.% of $FeCl_3 \cdot 6H_2O$ sintered at 800 °C particles used as adsorbent are 5.87, 5.82, 6.36, and 5.85, respectively.

The XRD diffractograms of the synthesized alumina-iron oxide doped particles after heat treatment at different temperatures are shown in Fig. 5 and characteristic phases are marked. The dominant structure in the synthetized alumina-iron oxide doped particles, with the adition of 4 wt.% of $FeCl_3 \cdot 6H_2O$, sintered at 700 and 800 °C is η – Al_2O_3 (PDF-1 77-0396) and for sintered at 900 °C, the dominant phases are η – Al_2O_3 (PDF-1 80-0955) and α – Al_2O_3 (PDF-1 75-1862). The ferrous oxide was added in 4 wt.% to alumina to ease the formation of corundum structure and this is visible from diffractograms where with the addition of ferrous oxide the temperature transformation lowers. On the other hand for adsorption, the structure having less crystallized structure could be more attractive. The addition of 13 wt.% in our experiments, gives the structure where hematite appears independently, as visible in Fig. 5. So in the specimen having 13 wt.% of added iron salt sintered at 800 °C, it is obvious that the hematite structure dominates and alumina is visible only as η alumina and the dominant structure is hematite that forms on lower temperatures. This material should have better properties in adsorption since this is a promising structure to be used in dye removal systems [26, 27].

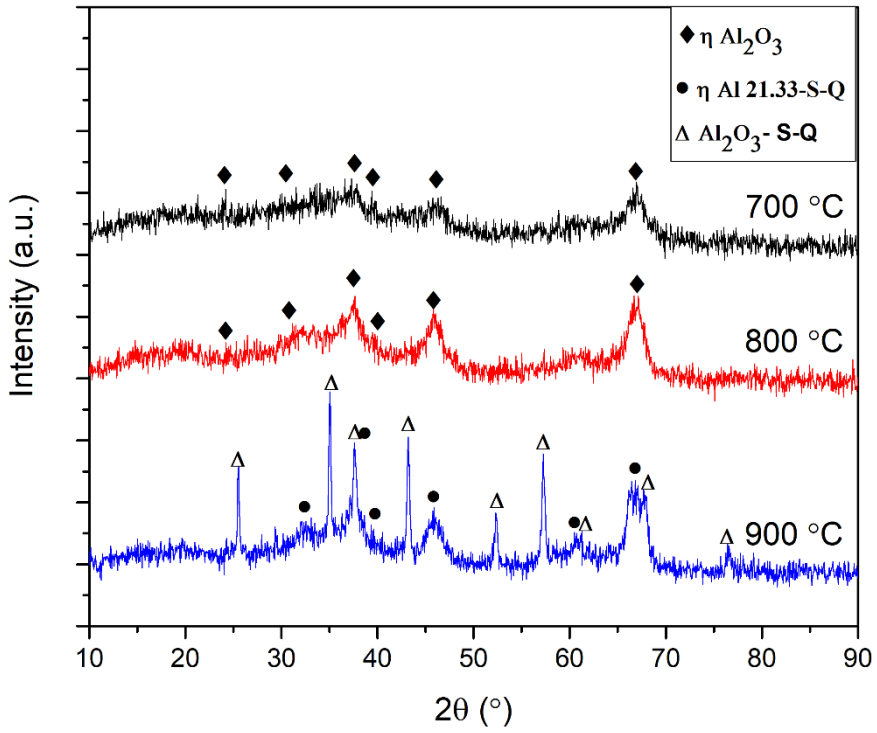

Fig. 5. XRD diffractogram of the synthesized alumina-iron oxide doped particles (with the adition of 4 wt.% of $FeCl_3 \cdot 6H_2O$) particles after heat treatment at different temperatures.

Fig. 6 shows the XRD diffraction patterns of alumina-iron oxide doped particles synthesized via heat treatment at 800 °C with 13 wt.% of $FeCl_3 \cdot 6H_2O$. The dominant phases in these particles are η – Al_2O_3 (PDF-177-0396) and α – Fe_2O_3 (PDF-164-0307).

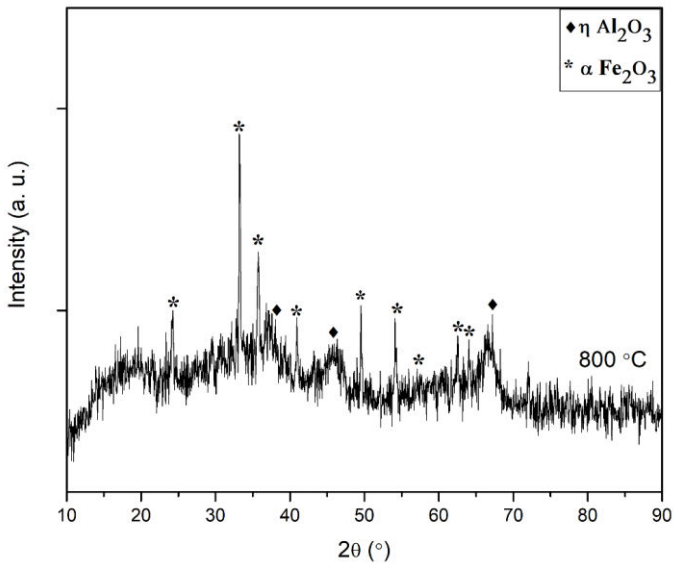

Fig. 6. XRD diffractogram of the synthesized η Al_2O_3 - α Fe_2O_3 particle after heat treatment at 800 °C showing the hematite structure that dominates.

3.2. Optimization of adsorption conditions

Many factors affect dye adsorption processes such as the initial concentration of adsorbent and dye, solution pH and temperature. Optimization of the mentioned conditions will greatly help in the development of dye removal from wastewater. In the further section, factors affecting dye adsorption are discussed.

The results of this study obtained by kinetics experiments were analyzed using the pseudo-first-order, pseudo-second-order adsorption rate model and intra-particle diffusion model since these models have been found to describe the sorption kinetics in anthraquinone dye sorption studies. The used kinetic models as presented by Equations 3-5, and summarized in Table I [28-30].

Tab. I Kinetics models for the description of the sorption kinetics in anthraquinone dye sorption studies.

model	Equation		Plot
Pseudo-first-order	$\ln(q_e - q_t) = lnq_e - \frac{k_1}{2.303}t$	(3)	$\ln(q_e - q_t)\ vs\ t$
Pseudo-second-order	$\frac{t}{q_t} = \frac{1}{k_2 q_e^2} + \frac{1}{q_e}t$	(4)	$\frac{1}{q_t}\ vs\ t$
Intra-particle diffusion	$-\ln\left(1 - \frac{q_t}{q_e}\right) = k_{dif}t$	(5)	$q_t\ vs\ t^{0.5}$

where k_1 (1/min), k_2 (g/(mg min)) and k_{dif} are the rates of constant of the pseudo-first-order, pseudo-second-order and intra-particle diffusion rate constant, respectively. Parameters q_t and q_e are adsorbed amount of dye during time and at equilibrium, respectively.

The obtained kinetics parameters for anthraquinone dye AB111 using the pseudo-first-order, pseudo-first-order kinetics model, and intra-particle diffusion model are presented in Table IIa-b, and kinetics plots for all three kinetics models are presented in the supplementary material (Figs S1-S10).

Tab. IIa The kinetics parameters for the AB111 adsorption using alumina-iron oxide doped particles sintered at 800 °C with addition of 4 wt.% of $FeCl_3 \cdot 6H_2O$

[Adsorbent] g/L	[AB111] mg/L	pH	Pseudo-first order			Pseudo-second order		
			q_e mg/g	k_1 1/min	R^2	q_e mg/g	k_2 g/(mg min)	R^2
0.5	100	3	2.58	0.011	0.9627	15.89	0.009	0.9987
0.75			1.98	0.016	0.9787	11.29	0.034	0.9996
1.0			1.53	0.015	0.9818	8.62	0.059	0.9998
1.25			1.30	0.013	0.9949	7.09	0.079	0.9999
1.5			1.16	0.016	0.9802	5.97	0.126	1
1.0	25	3	1.09	0.002	0.8852	2.31	0.260	0.9999
	50		1.15	0.009	0.9472	4.56	0.160	0.9997
	75		1.26	0.010	0.9931	6.25	0.078	0.9997
	100		1.53	0.015	0.9818	8.62	0.059	0.9999
1.0	100	2.5	1.45	0.013	0.9846	8.33	0.059	0.9998
		3.0	1.53	0.015	0.9818	8.62	0.060	0.9999
		3.5	1.75	0.008	0.9940	6.58	0.018	0.9945
		4.0	0.85	0.008	0.9614	6.37	0.011	0.9903
		6.8	1.72	0.010	0.9887	4.92	0.010	0.9907

Tab. IIb The kinetics parameters for the AB111 adsorption using alumina-iron oxide doped particles sintered at 800 °C with addition of 4 wt.% of $FeCl_3 \cdot 6H_2O$

[Adsorbent] g/L	[AB111] mg/L	pH	Interparticle diffusion					
			k_1	C_1	R^2	k_2	C_2	R^2
0.5	100	3	2.793	0.096	0.9871	0.581	9.726	0.9999
0.75			0.739	6.510	0.9868	0.217	9.184	0.9143
1.0			0.672	4.947	0.9936	0.142	7.288	0.9472
1.25			0.427	4.604	0.9985	0.113	6.046	0.9764
1.5			0.350	4.087	0.9465	0.074	5.286	0.9359
1.0	25	3	0.107	1.646	0.9837	0.039	1.959	0.9634
	50		0.208	3.350	0.9699	0.069	3.943	0.9828
	75		0.337	4.077	0.9366	0.160	4.928	0.9998
	100		0.672	4.947	0.9936	0.142	7.288	0.9475
1.0	100	2.5	0.552	5.091	0.9903	0.115	7.167	0.9943
		3.0	0.672	4.947	0.9936	0.142	7.288	0.9472
		3.5	0.746	1.197	0.9909	0.449	2.440	0.9944
		4.0	0.740	0.228	0.9956	0.361	2.399	0.9415
		6.8	0.660	0.454	0.9559	0.351	1.014	0.9989

Analyzing the results of kinetics study for all initial conditions and comparison of pseudo-first-order and pseudo-second-order kinetics model experimental data shows a good fitting with the pseudo-second-order kinetics model with a high value of R^2 (>0.99). The experimental data obtained by the intra-particle diffusion model confirm the multi-step mechanism of AB111 adsorption. The intra-particles diffusion plot (Figs S3, S6, and S9, Supplementary material) shows two steps of dye adsorption. In the first 20 minutes of adsorption, the process has a higher value of kdif1 which corresponds to superficial adsorption, after 20 minutes of the dye adsorption process, the values of k_{dif2} are decreased which corresponds to subsequent intraparticle or pore diffusion. The value of C1 and C2

shows that the plots do not pass through origin which contributes to the intra-particle is not the singular determining step.

3.2.1. The influence of the initial adsorbent concentration

The effect of the initial alumina-iron oxide doped particles sintered at 800 °C with 4 wt.% of iron salt, concentration was studied at a constant dye concentration, temperature, and pH value. In this part of the experiment, the initial adsorbent concentration was in the range 0.5-1.5 g/L. Fig. 7 shows the percentage of dye removal versus time for different initial adsorbent concentration and the red scale shows the dependence of adsorption capacity from initial adsorbent concentration.

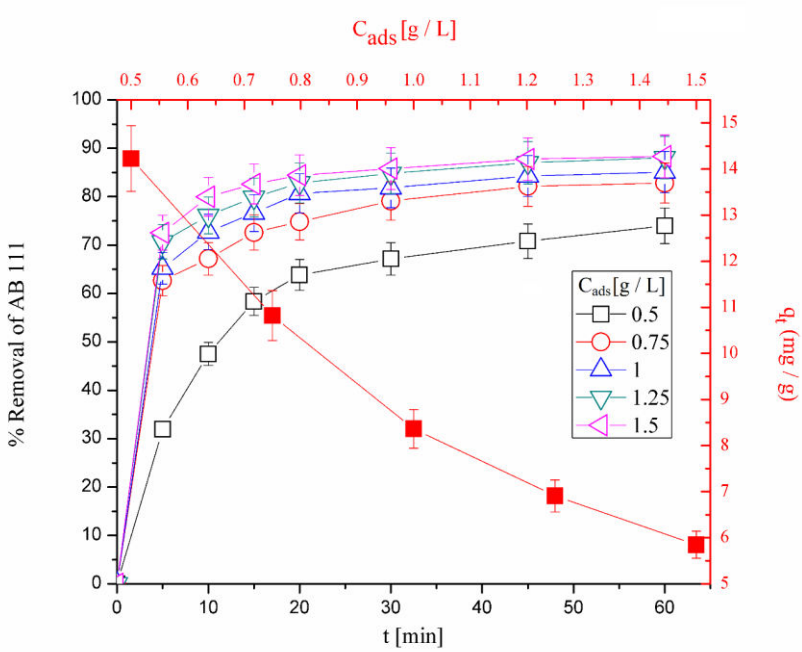

Fig. 7. The percentage of dye removal versus time for different initial adsorbent concentration (black scale) and the dependence of adsorption capacity from initial adsorbent concentration (red scale). Initial conditions: C_{AB111}= 100 mg/L, pH= 3, T= 293.15 K, ω= 750 rpm. Alumina-iron oxide doped particles sintered at 800 °C with 4 wt.% of iron salt were used.

As can be seen from Fig. 7 the adsorption capacity and dye removal depend on the initial concentration of the alumina-iron oxide doped particles sintered at 800 °C with 4 wt.% of $FeCl_3 \cdot 6H_2O$. The increasing of the adsorbent concentration initiates the decrease of the adsorption capacity and increasing the percentage of dye removal. In the system in which was used the lowest concentration of adsorbent (0.5 g/L), obtained adsorption capacity was 14.22 mg/g and after 60 minutes was removed 73.9 % of dye. Opposite the system with the lowest initial adsorbent concentration, increasing the adsorbent concentration to 1.5 g/L, adsorption capacity is decreased to 5.85 mg/g and the percentage of dye removal is increased to 88.3 %. The adsorption rate in the system with the lowest adsorption concentration was k_2= 0.009 g/(mg min). The increase in adsorbent concentration, increase the adsorption rate. Thus, in the system with the highest concentration, the adsorption rate was k_2= 0.126 g/(mg min) (Table II, and Figure S2, Supplementary material). The explanation for this phenomenon is that increase in the amount of adsorbent initiate the increase in the quantity of sorption sites at the adsorbent surface and enable the higher percentage of dye removal. From an economical point of view, the basic idea is to use the smallest amount of adsorbent for decreasing dye

concentration to lower concentration than those prescribed by law which describes pollutant concentration in water [31].

3.2.2. The influence of the initial dye concentration

The percent of dye removal is highly dependent on the initial dye concentration. The effect of initial dye concentration depends on the immediate relation between the concentration of the dye and the available sites on an adsorbent surface [2]. The influence of the initial dye concentration was investigated in the range 25-100 mg/L under the same conditions, and as an adsorbent was used alumina-iron oxide doped particles with 4 wt.% of $FeCl_3 \cdot 6H_2O$ sintered at 800 °C. The percentage of dye removal versus time for different initial dye concentration is shown in Figure 8, and the red scale of the same figure donates the dependence of adsorption capacity at different initial dye concentrations.

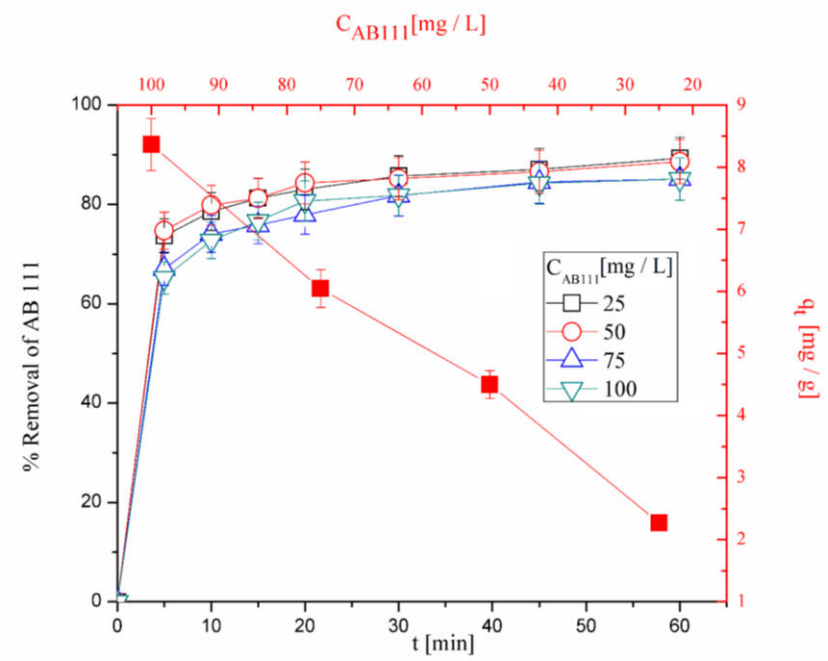

Fig. 8. The the percentage of dye removal versus time for different initial dye concentration (black scale) and the dependence of adsorption capacity from initial dye concentration (red scale). Initial conditions: C_{ads}= 1g/L, pH= 3, T= 293.15 K, ω= 750 rpm. Alumina-iron oxide doped particles sintered at 800 °C with 4 wt.% of iron salt were used.

According to the results presented in Fig. 8, it can be concluded that the increase of the initial dye concentration causes the decrease of dye removal, which may be due to the saturation of adsorption sites on the adsorbent surface. Also, the increase of the initial dye concentration will cause an increase in the capacity of the adsorbent and this may be due to the high driving force for mass transfer at a high initial dye concentration [32]. In the system with initial dye concentration 25 mg/L 89.2 % of dye was removed, adsorption constant was 2.27 mg/g and the adsorption rate was k_2= 0.26 g/(mg min) (Table II, and Fig. S5, Supplementary material). An increase of the initial dye concentration to 100 mg/L decreases the percentage of dye degradation to 85.1 %, adsorption constant was 8.36 mg/g and the adsorption rate was k_2= 0.059 g/(mg min) (Table II., and Fig. S5, Supplementary material).

Mahapatra et al. [26] studied the adsorption of Congo Red by iron oxide – alumina nanocomposites and they found that when the Congo Red concentration increased from 20

mg/L to 1000 mg/L using α-Fe_2O_3–Al_2O_3 and γ-Fe_2O_3–Al_2O_3 almost 100 % of dye was adsorbed [27]. Banerjee et al. [33] studied the removal of Orange G from aqueous solution by adsorption process using alumina nanoparticles. They showed that increasing dye concentration decreases the percentage of removal. In the system where the dye concentration was 50 mg/L cca. 95 % was removed while increase of initial dye concentration to 125 mg/L decreases the percentage of dye removal after 120 minutes to cca. 75 %.

3.2.3. The effect of the initial pH value

Besides the effect of the initial dye and adsorbent concentration and temperature, the pH value of the solution is very important for the adsorption. The influence of initial pH value was investigated in the range 2.5 – 7.4 (pH value of dye solution) pH value. The alumina-iron oxide doped particles with 4 wt.% of $FeCl_3 \cdot 6H_2O$ sintered at 800 °C were used as adsorbent. The percentage of dye removal efficiency versus time for different pH values (black scale) and the dependence of adsorption capacity from initial pH value (red scale) are presented in Fig. 9.

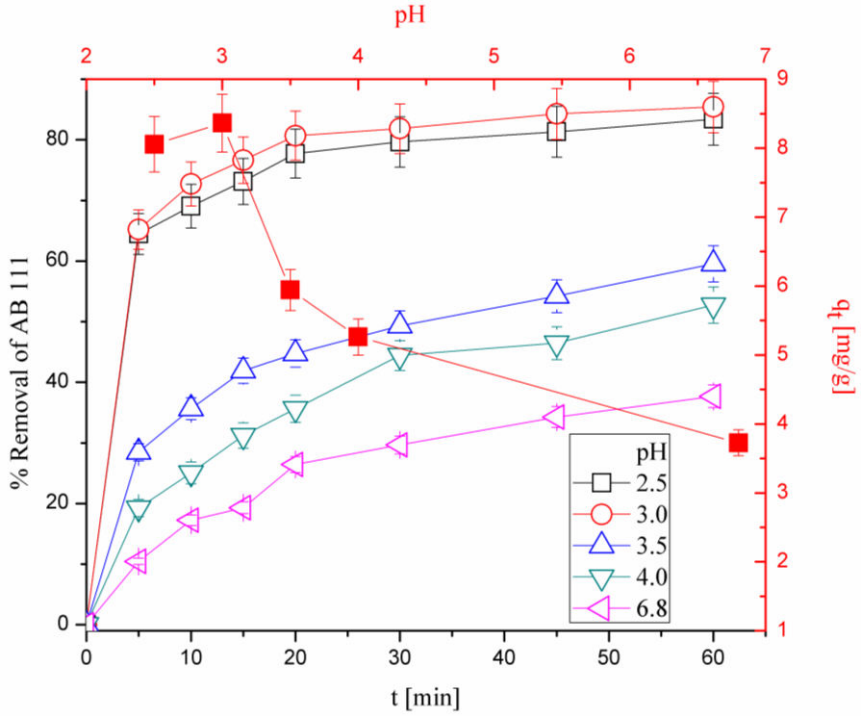

Fig. 9. The percentage of dye removal versus time for different pH values (black scale) and the dependence of adsorption capacity from initial pH value (red scale). Initial conditions: C_{AB111}= 100 mg/L, C_{ads}= 1 g/L, T= 293.15 K, ω= 750 rpm. Alumina-iron oxide doped particles sintered at 800 °C with 4 wt.% of iron salt were used.

The results presented in Fig. 9 prove that the pH value is important for effective adsorption of AB111. At pH range 2.5-3 adsorption capacities are higher than in the near-neutral state. The highest values of adsorption capacity (q_t = 8.36 mg/g) and the percentage of dye removal (85.4 %) obtained at pH 3. Further increasing of pH value causes the decrease of adsorption capacity and the percentage of dye removal, at dye pH value (pH 6.8) adsorption capacity and the percentage of dye removal were decreased to q_t = 3.73 mg/g and 37.7 % of removed dye. Adsorption rates are in agreement with the adsorption capacity and the dye removal efficiency trends. Thus, the adsorption rate in the most effective system (pH 3) was

k_2= 0.60 g/(mg min) while at pH value of dye, the adsorption rate was k_2= 0.010 g/(mg min). The pseudo-second-order kinetics plot is presented in Table IIa-b, and Supplementary material, Fig. S8. The adsorbent surface in the neutral and basic medium becomes negatively charged due to the deprotonation and the adsorption of anionic dye ions gets severely hindered as a result of columbic repulsion. In acidic pH conditions, when the pH value is lower than pH_{zpc}, the alumina surface contains a large number of positively charged electrostatically binding sites and attracted the anionic AB111 species and leads to the higher efficiency of the dye adsorption [33]. Hence, the system with pH 2.5 was more effective for AB111 removal than the system without adjusting pH value (pH 6.8). A similar observation has been reported for adsorption of acid dyes Methyl Orange [34] and Orange G [35].

3.2.4. The comparison of adsorbents efficiency

The temperature of sintering is an important parameter for alumina-iron oxide doped particle preparation since it can affect the particles structure. The dye adsorption effectiveness of alumina-iron oxide doped particles with 4 wt.% of $FeCl_3 \cdot 6H_2O$ synthesized at three different temperatures (700, 800 and 900 °C) with the addition of 4 wt.% of $FeCl_3 \cdot 6H_2O$ and alumina particles doped with Fe_2O_3 at 800 °C of heating temperature with addition of 13 wt.% of $FeCl_3 \cdot 6H_2O$. Fig. 10 shows the adsorption capacities and dye removal efficiency for different type's alumina-iron oxide doped particles.

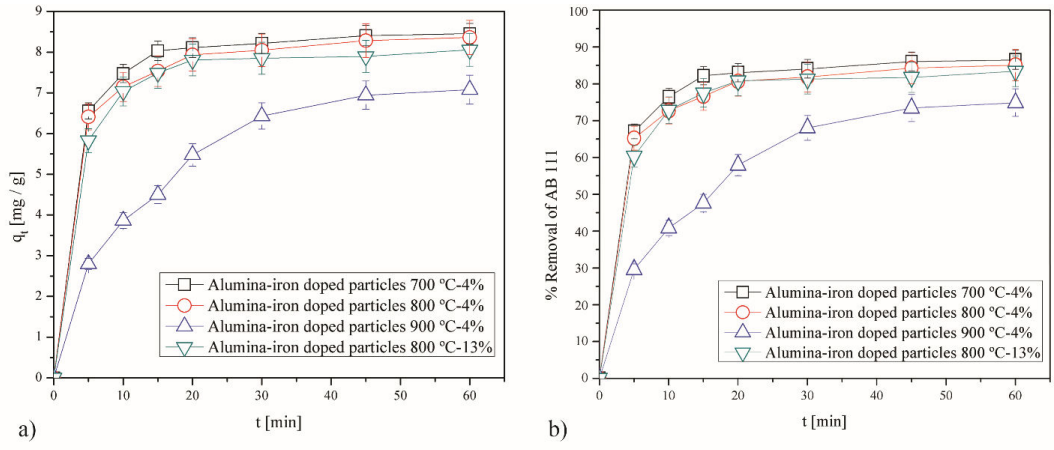

Fig. 10. The dependence of adsorption capacity from the type of adsorbent particles (a) and the percentage of dye removal versus time for a different type of adsorbent (b). Initial conditions: C_{AB111}= 100 mg/L,C_{ads}= 1 g/L, T= 293.15 K, ω= 750 rpm.

The obtained results (Fig. 10) shows that the alumina-iron oxide doped particles synthesized at 700 °C with lower iron salt concentration have the highest adsorption capacity (8.45 mg/g). After 60 minutes, using the same adsorbent, 87.5 % of dye was absorbed. Increase of sintering temperature up to 900 °C, causes the decrease of adsorption capacity to 7.08 mg/g and the efficiency of dye removal to 74.8 %. Similar trend is observed with the adsorption rate. The adsorption rate of adsorbent material synthesized at 700 °C is higher (k_2= 0.083 g/(mg min)) than one of the alumina-iron oxide doped particles synthesized at 900 °C (k_2= 0.01 g/(mg min)) (Fig. S10, Supplementary material). The sample of the alumina-iron oxide doped particles sintered at 800 °C with 4 wt.% of $FeCl_3 \cdot 6H_2O$ has lower adsorption capacity and the efficiency of dye removal than the sample at 700 °C (less than 5 %). These samples have similar structures while the structure of the sample at 800 °C and 13 wt.% of $FeCl_3 \cdot 6H_2O$ has hematite in its structure. This change in the structure additinally lowered the adsorption capacity of the adsorbent but the efficiency of dye removal is similar to the sample

with less iron in the structure. The adsorption capacity of the particles sintered at 800 °C with 13 wt.% of $FeCl_3 \cdot 6H_2O$ was q_t = 8.05 mg/g, and the 83.4 % of initial dye concentration was effectively adsorbed. This implies that the formation of α–Al_2O_3 lowers the adsorption capacity and the efficiency of dye removal more than the formation of α-Fe_2O_3. Since there was not much difference between samples sintered with 4 and 13 wt.% of $FeCl_3 \cdot 6H_2O$, we decided to work father with the particles with less iron in the structure.

3.2.5. Adsorption isotherms

For the design of the adsorption system, the equilibrium adsorption isotherm is valuable data that describes the way of interaction between adsorbates and adsorbents. Two important isotherm models were used to determine if the adsorbent surface during the process of dye adsorption: Langmuir [35] and Freundlich isotherms [36]. The Langmuir adsorption isotherms have been used successfully for many adsorption processes of monolayer adsorption, while the Freundlich isotherm describes the adsorption characteristics for multilayer adsorbent surface [36]. The isotherms factors were evaluated at pH 3 for describing alumina-iron oxide doped particles sintered at 800 °C with 4 wt.% of $FeCl_3 \cdot 6H_2O$ surface.
The equation for the Langmuir model for alumina is described by Equation 6 [37]:

$$q_t = \frac{q_m K_L C_t}{1 + K_L C_t} \qquad (6)$$

where C_t (mg/L) represents concentration of AB111 in solution at equilibrium, mass of adsorbed dye per gram of alumina at equilibrium is presented by symbol q_t (mg/g), constant related to monolayer adsorption capacity of alumina is q_m (mg/g) and K_L (L/mg) is the Langmuir constant. A non-linear plot of q_t versus C_t (Fig. 11) gives the values of constants q_m and K_L.

The presented results in Fig. 11 show the high values of correlation factors (R^2>0.99). The values of the all-important Langmuir isotherm model parameters are presented in Table III. The obtained values of the Langmuir constant and q_m show high dependence of temperature. Increase in temperature increase the Langmuir constant and q_m.

The separation factor, R_L, is a dimensionless constant and can be used to explain the essential characteristics of the Langmuir equation. R_L is defined as Equation 7 [17][38]:

$$R_L = \frac{1}{1 + K_L C_t} \qquad (7)$$

where K_L and C_t are explained in the previous equation. Acceptability of the adsorption process is depending on the value of the separation factor. The adsorption process is only favorable if $0 < R_L < 1$ [39]. The dependence of the separation factor on the initial dye concentration is presented in Fig. 12.

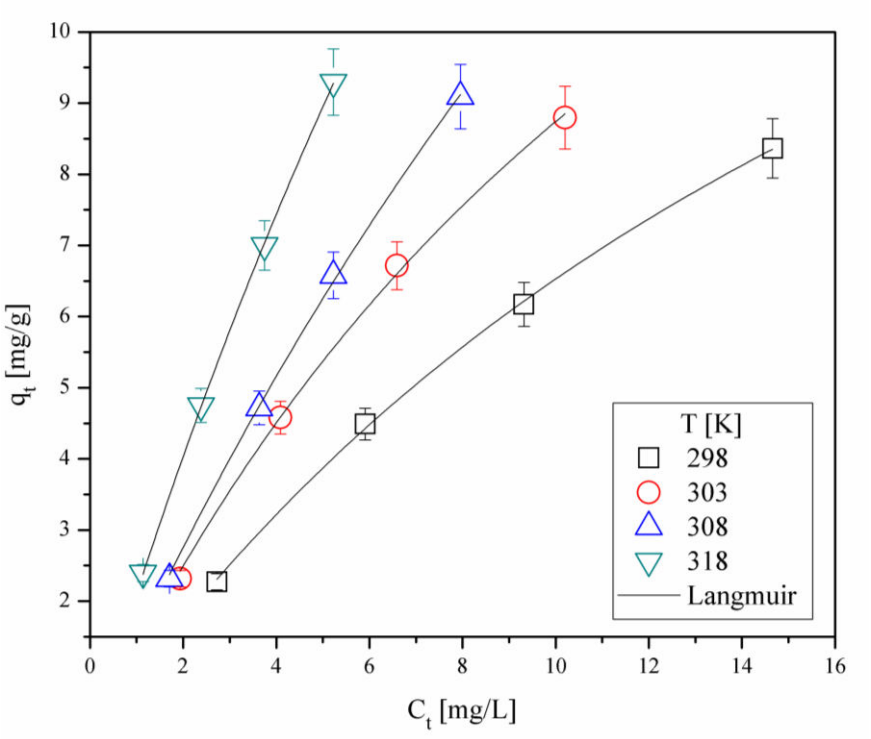

Fig. 11. Langmuir adsorption isotherm plot for removal of AB111. Initial conditions:C_{ads}= 1 g/L, pH= 3, ω= 750 rpm. Alumina-iron oxide doped particles sintered at 800 °C with 4 wt.% of iron salt were used.

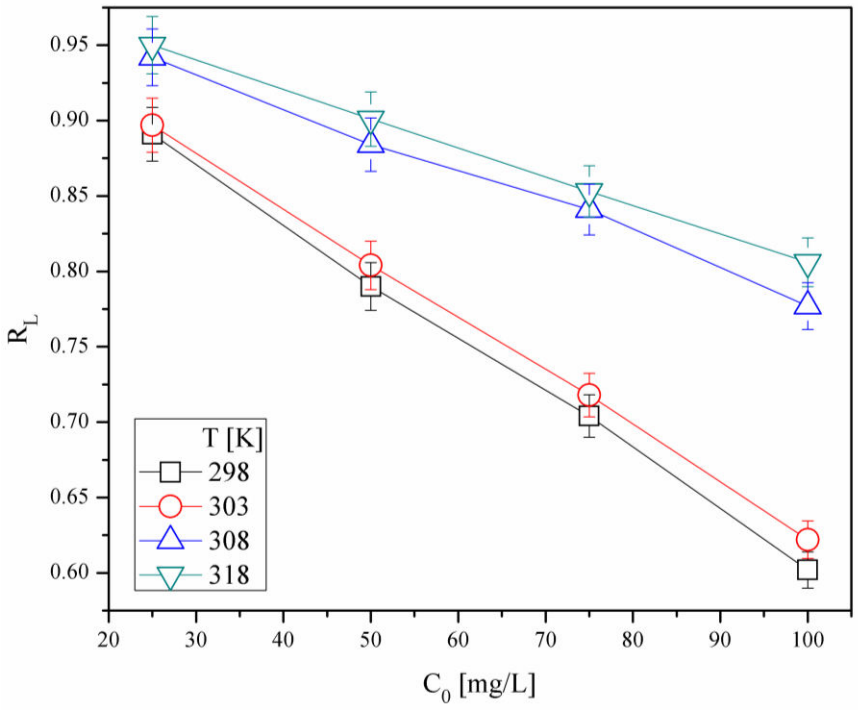

Fig. 12. The dependence of separation factor R_L on the initial concentration of AB111. Initial conditions: C_{ads}= 1 g/L, pH= 3, ω= 750 rpm. Alumina-iron oxide doped particles sintered at 800 °C with 4 wt.% of iron salt were used.

The results presented in Fig. 12 shows that the decrease of the separation factor follows the increase of the initial dye concentration which indicates that the adsorption on alumina particles are more favorable at higher values of temperature and the initial concentration of dye parameters. Also, the values of the separation factor are in the range between 0 and 1 which leads to a conclusion that adsorption of AB111 onto alumina surface corresponds to the Langmuir adsorption isotherm model as a better fitting model and the used alumina-iron oxide doped particles are adsorbent with homogenous surface. Also, dye particles form monolayer on adsorbent surface.

Describing the adsorption characteristics for heterogeneous adsorbent surface by Freundlich adsorption isotherm can be expressed mathematically by Equation 8 as [34]:

$$q_t = K_F C_t^{1/n} \quad (8)$$

where q_t and C_t are described earlier, K_F is a constant representing the adsorbent capacity and 1/n is a constant heterogeneity factor. These factors characteristics for Freundlich isotherm are determined from non-linear function. The numerical value of exponent 1/n < 1 shows that Freundlich adsorption isotherm is favorable [34]. The experimental results for Freundlich adsorption isotherms fitting investigation are presented in Table III. The Freundlich adsorption isotherm plot for removal of AB111 by alumina-iron oxide doped particles dried at 800 °C with 4 wt.% of $FeCl_3 \cdot 6H_2O$ adsorbent is presented in Fig. 13.

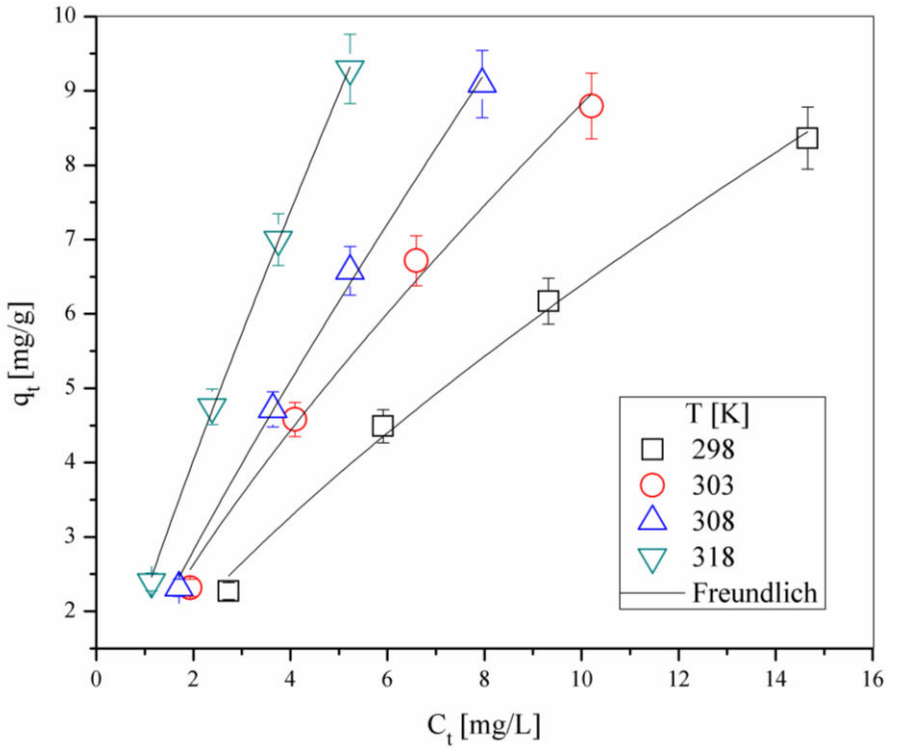

Fig. 13. Freundlich adsorption isotherm plot for removal of AB111. Initial conditions: C_{ads}= 1 g/L, pH= 3, ω= 750 rpm. Alumina-iron oxide doped particles sintered at 800 °C with 4 wt.% of iron salt were used.

According to the results presented in Fig. 13, Freundlich adsorption isotherm plot has correlation factor (R^2>0.99) similar to the Langmuir adsorption isotherm plot. The obtained values of K_L, 1/n, and R^2 are presented in Table III.

Tab. III Langmuir and Freundlich adsorption isotherm constants for the adsorption of AB111 onto alumina-iron oxide doped particles sintered at 800 °C with 4 wt.% of $FeCl_3 \cdot 6H_2O$.

Temperature (K)	Langmuir adsorption isotherm					Freundlich adsorption isotherm		
	K_L (L/mg)	q_m (mg/g)	C_0 (mg/L)	R_L	R^2	K_F	1/n	R^2
298	0.045	20.85	25	0.891	0.9943	1.187	0.7309	0.9942
			50	0.790				
			75	0.704				
			100	0.602				
303	0.0595	23.44	25	0.897	0.9983	1.563	0.7515	0.9894
			50	0.804				
			75	0.718				
			100	0.622				
308	0.036	32.15	25	0.942	0.9992	1.556	0.856	0.9965
			50	0.884				
			75	0.841				
			100	0.777				
318	0.046	44.84	25	0.950	0.9998	2.1996	0.8731	0.9996
			50	0.901				
			75	0.853				
			100	0.806				

Results presented in Table III shows that Langmuir adsorption isotherm is favorable ($0 < R_L < 1$) and the obtained values of the Langmuir constant and q_m show high dependence of temperature. According to the values of the Langmuir constant and q_m, the increase of temperature has a favorable effect on dye adsorption onto alumina particles. On the other side, the values of 1/n from Table III ($1<1/n$) prove that the Freundlich adsorption isotherm is not favorable. Langmuir and Freundlich adsorption isotherm parameters presented in Table III lead to the conclusion that the alumina-iron oxide doped particles sintered at 800 °C with 4 wt.% of $FeCl_3 \cdot 6H_2O$ is adsorbent with a homogenous surface and adsorption process form a monolayer coverage of dye particles onto adsorbent. Due to the homogeneous surface of the adsorbent, it is not possible to calculate the free energy and porosity using the Dubinin-Radushcevich izotherm model [40].

3.2.6. Thermodynamic study

Additionally, the thermodynamics study was performed and enthalpy (ΔH°), entropy (ΔS°), and Gibbs free energy (ΔG°) of the adsorption of AB111 onto the alumina adsorbent were determined. The thermodynamic parameters can be described by the following Equations 9-11 [41-43]:

$$K_0 = \frac{(C_0 - C_t)m}{C_0 V} \quad (9)$$

$$lnK_0 = -\frac{\Delta G^0}{RT} = \frac{\Delta S^0}{R} - \frac{\Delta H^0}{RT} \quad (10)$$

$$\Delta G^0 = -\mathrm{RT}\ln K_0 \quad (11)$$

where m is adsorbent weight, V is volume of system, R is the universal gas constant, T is the absolute temperature of the reaction solution expressed in Kelvin and K_0 is distribution coefficient. Thermodynamics parameters ΔH^o and ΔS^o can be calculated from the slope and

intercept of values of distribution coefficients plotted against *1/T*. The value of ΔG^o can be calculated from Equation 11. The calculated thermodynamic parameters are listed in Table IV. In thermodinamics study, alumina-iron oxide doped particles sintered at 800 °C with addition of 4 wt.% of $FeCl_3 \cdot 6H_2O$ were used.

Tab. IV The calculated thermodynamic parameters for dye adsorption process. Initial conditions: C_{ads}=1 g/L,C_{AB111}=100 mg/L, pH= 3, ω = 750 rpm.

Temperature [K]	K_0[mg/L]	ΔG^o [kJ/mol]	ΔH^o [kJ/mol]	ΔS^o [J/mol K]
298	0.058	-23.8	-36.8	-43.7
303	0.087	-23.6		
308	0.115	-23.4		
318	0.181	-22.9		

The negative value of Gibbs free energy and its slight increase caused by increase of temperature shows that the dye adsorption process is spontaneous and increase the feasibility of adsorption at higher temperatures. The negative value of enthalpy confirms the exothermic nature of dye adsorption onto alumina-iron oxide doped particles. Also, according to the previous investigations, the value of enthalpy is lower than 40 kJ/mol which corresponds to the physical adsorption mechanism [34, 43]. The value of $\Delta S°$ can be used to describe the decreasing of the randomness at the solution made ofadsorbent/adsorbate system during dye adsorption [45]. The values of the K_0 presented in Table IV shows that the mobility of particles in the system increases with increase of temperature [44].

3.3. FT-IR spectroscopy

The assessment of alumina-iron oxide doped particlesurfaces and dye functional groups after adsorption was carried out by FT-IR spectral analysis. The FT-IR spectra of alumina-iron oxide doped particles synthesized in this work are given in Fig. 14a. Also, the FT-IR spectra of alumina-iron oxide doped particles sintered at 800 °C with the addition of 4 wt.% of $FeCl_3 \cdot 6H_2O$ before and after adsorption as well FT-IR spectra of AB111 are shown in Fig. 14b.

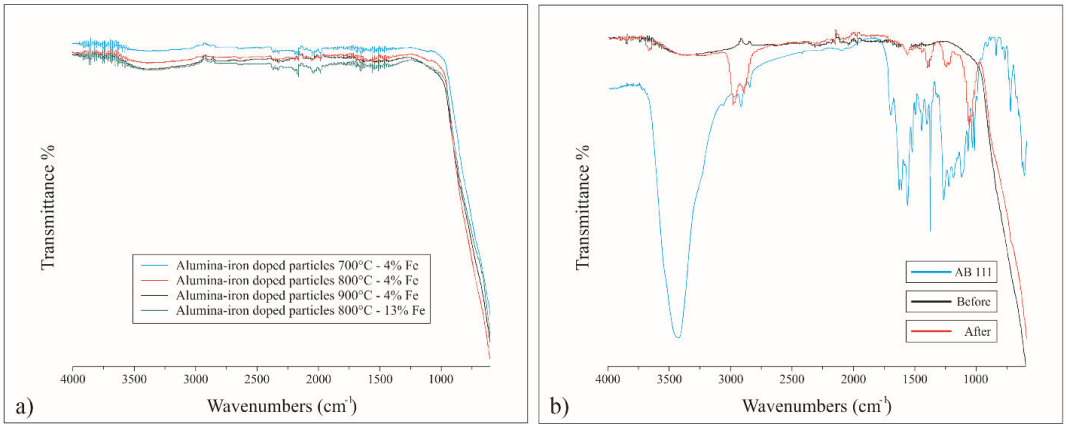

Fig. 14. FT-IR spectra of alumina-iron oxide doped particles sintered at different conditions (marked in Fig.) (a) and FT-IR spectra of AB111 and alumina-iron oxide doped particles with the addition of 4 wt.% of $FeCl_3 \cdot 6H_2O$ sintered at 800 °C surface before and after adsorption (b).

Peaks in the range 2966-3550 cm^{-1}, which belongs to the stretching vibrations of OH functional group, were observed in the FT-IR spectra of alumina particles (Fig.14a). In the rest of FT-IR spectra, a wide peak in wavenumbers range 500-1000 cm^{-1} that can be assigned to Al–O bonds, can be noticed. Also, in this range, peaks can be originated by octahedral (>700 cm^{-1}) and tetrahedral structure of Al^{3+} (700-950 cm^{-1}) [22].

The anthraquinone dye AB111 was analyzed earlier by FT-IR spectral analysis and results were presented by Stupar et al. [7]. Fig. 14b shows the FT-IR spectra of adsorbent before and after dye adsorption. The changes in FT-IR spectra after adsorption observed at range 3700 to 3300 cm^{-1} can be assumed to –ON and $–NH_2$ vibrations. The peaks observed at 2922 and 2855 cm^{-1} can be attributed to C-H aliphatic vibrations which belong to adsorbed dye. The peaks at 1698 and 1628 cm^{-1} belong to C=O ester and C=O vibrations, respectively. The peak observed at 1382 cm^{-1} originated in CH_3 vibrations. Also, peaks at 1273 and 1076 cm^{-1} can be attributed to C–O and $–SO_3H$, respectively [7]. Enumerated changes of FT-IR spectra show the surface modification as a result of the dye adsorption.

4. Conclusion

Adsorption of anthraquinone dye AB111 from aqueous solutions was studied using alumina-iron oxide doped particles sintered at different temperatures (700, 800, and 900 °C) with the addition of 4 wt.% of $FeCl_3 \cdot 6H_2O$ as well as with the addition of 13 of wt.% of the same salt (800 °C). The morphology and the structure of samples were examined by SEM analyses. The distribution of alumina-iron oxide doped particles sintered at 800 °C with lower mass of iron salt is mostly in the range 0.5-0.7 μm, and for particles sintered at the same temperature with higher mass of iron salt is smaller (0.1-0.2 μm). The XRD analysis showed that the dominant structure in the synthetized alumina-iron oxide doped particles, with the adition of 4 wt.% of $FeCl_3 \cdot 6H_2O$, sintered at 700 and 800 °C is $\eta - Al_2O_3$ and for sintered at 900 °C, the dominant phases are $\eta - Al_2O_3$ and $\alpha - Al_2O_3$. The samples sintered at 800 °C with 13 wt.% of $FeCl_3 \cdot 6H_2O$ have as the dominant phases $\eta - Al_2O_3$ and $\alpha - Fe_2O_3$. The adsorption kinetics can be satisfactorily described by the pseudo-second-order reaction rate model. By comparison of samples, the alumina-iron doped particles sintered at 700 °C with 4 wt.% of iron salt have the highest efficiency in AB111 removal by adsorption (87.5 %). The increase of temperature of sintering causes the decreasing of dye adsorption efficiency. The increase of $FeCl_3 \cdot 6H_2O$ during the preparation of adsorbent leads to the change in the structure which additinally lowers the adsorption capacity but the efficiency of dye removal is similar. The experimental data shows good fitting with Langmuir isotherm which confirms that the surface of adsorbent is homogenous and at equilibrium, dye particles form monolayer on adsorbent surface. According to the obtained thermodynamic parameters, adsorption of anthraquinone dye AB111 onto alumina-iron oxide doped particles is a spontaneous physisorption process with exothermic nature.

Acknowledgments

The Ministry of Education, Science and Technological Development of the Republic of Serbia have financed this research (Contract No. 451-03-68/2020-14/200135). We are thankful to prof Enis Dzunuzovic for valuable coments and suggestions.

5. References

1. W. S. W. Ngah, L. C. Teong, M. A. K. M. Hanafiah, Adsorption of dyes and heavy metal ions by chitosan composites: A review, Carbohydr. Polym. 83 (2011) 1446-

1456.
2. L. A. V. de Luna, T. H. G. da Silva, R. F. P Nogueira, F. Kummrow, G. A. Umbuzeiro, Aquatic toxicity of dyes before and after photo-Fenton treatment, J. Hazard. Mater. 276 (2014) 332-338.
3. R. O. A. de Lima, A. P. Bazo, D. M. F. Salvadori, D. M. Rech, D. P oliveira, G. A. Umbuzero, Mutagenic and carcinogenic potential of a textile azo dye processing plant effluent that impacts a drinking water source, Mutat. Res.-Gen. Tox. En. 626 (2007) 53-60.
4. F. Zaviska, P. Drogui, J. F. Blais, G. Mercier, In situ active chlorine generation for the treatment of dye-containing effluents, J. Appl. Electrochem. 39 (2009) 2397-2408.
5. I. Belbachir, B. Makhoukhi, Adsorption of Bezathren dyes onto sodic bentonite from aqueous solutions, J. Taiwan Inst. Chem. Eng. 75 (2017) 105-111.
6. A. A. Oladipo, M. Gazi, S. Saber-Samandari, Adsorption of anthraquinone dye onto eco-friendly semi-IPN biocomposite hydrogel: Equilibrium isotherms, kinetic studies and optimization, J. Taiwan Inst. Chem. Eng. 45 (2014) 653-664.
7. S. L. Stupar, B. N. Grgur, A. E. Onjia, D. Mijin, Direct and indirect electrochemical degradation of acid blue 111 using IrOX anode, Int. J. Electrochem. Sci. 12 (2017) 8564-8577.
8. B. Gözmen, B. Kayan, A. M. Gizir, A. Hesenov, Oxidative degradations of reactive blue 4 dye by different advanced oxidation methods, J. Hazard. Mater. 168 (2009) 129-136.
9. A. Kausar, M. Iqbal, A. Javed, K. Aftab, Z. H. Nazli, H. N. Bhatti, S. Nouren, Dyes adsorption using clay and modified clay: A review, J. Mol. Liq. 256 (2018) 395-407.
10. C. Luca, F. Ivorra, P. Massa, R. Fenoglio, I. Fac, D. I. N. De Mar, J. B. Justo, Alumina Supported Fenton-Like Systems for the Catalytic Wet Peroxide Oxidation of Phenol Solutions, Ind. Eng, Chem. Res. 51 (2012) 8979-8984.
11. Y. Chen, D. Zhang, X. Wu, H. Wang, C. Zhang, W. Yang, Y. Chen, Epoxy/α-alumina nanocomposite with high electrical insulation performance, Prog. Nat. Sci. Mater. Int. 27 (2017) 574-581.
12. K. Ishaq, A. A. Saka, A. O. Kamardeen, A. Ahmed, M. I. Alhassan, H. Abdullahi, Characterization and antibacterial activity of nickel ferrite doped α-alumina nanoparticle, Eng. Sci. Technol. an Int. J. 20 (2017) 563-569.
13. K. Y. Paranjpe, Alpha, Beta and Gamma Alumina as a catalyst -A Review, Pharma Innovation 6 (2017) 236-238.
14. S. Perišić, M. M. Vuksanović, M. Petrović, A. Radisavljević, A. Grujić, R. M. Jančić-Heinemann, V. Radojević, Impact of Alumina Particles on the Morphology and Mechanics of Hybrid Wood Plastic Composite Materials, Sci. Sinter. 51 (2019) 115-124.
15. V. Gopalakannan, S. Periyasamy, N. Viswanathan, One pot eco-friendly synthesis of highly dispersed alumina supported alginate biocomposite for efficient chromium (VI) removal, J. Water Process Eng. 10 (2016) 113-119.
16. P. Milanović, M. M. Vuksanović, M. Mitrić, A. Kojović, D. Mijin, R. Jančić-Hainemann, Alumina Particles Doped With Ferric as Efficient Adsorbent for Removal of Reactive Orange 16 from Aqueous Solutions, 50 (2018) 467-476.
17. A. Wasti, M. A. Awan, Adsorption of textile dye onto modified immobilized activated alumina, J. Assoc. Arab Univ. Basic Appl. Sci. 20 (2016) 26-31.
18. R. Rehman, T. Mahmud, J. Anwar, M. Salman, Removal of Alizarin Red S (Dye) from Aqueous Media by using Alumina as an Adsorbent, J. Chem. Soc. Pak. 33 (2011) 228-232.
19. A. Drah, N. Tomić, Z. Veličić, A. D. Marinković, Ž. Radovanović, Z. Veličković, R. Jančić-Heinemann, Highly ordered macroporous γ -alumina prepared by a modified

sol-gel method with a PMMA microsphere template for enhanced Pb^{2+}, Ni^{2+} and Cd^{2+} removal, Ceram. Int. 43 (2017) 13817-13827.
20. A. A. Ashor, M. M. Vuksanović, N. Z. Tomić, A. Marinković, R. Jančić-Heinemann, The influence of alumina particle modification on the adhesion of the polyacrylate matrix composite films and the metal substrate, Compos. Interfaces. 26 (2019) 417-430.
21. S. L. Stupar, B. N. Grgur, M. M. Radišić, A. E. Onjia, N. D. Ivanković, A. V Tomašević, D. Ž. Mijin, Oxidative degradation of Acid Blue 111 by electro-assisted Fenton process, J. Water Process Eng. 36 (2020) 101394.
22. A. A. Algellai, N. Tomić, M. M. Vuksanovi, M. Dojčinović, T. Volkov-Husović, V. Radojević, R. Jančić-Heinemann, Adhesion testing of composites based on Bis-GMA/TEGDMA monomers reinforced with alumina based fillers on brass substrate, Compos. Part B. 140 (2018) 164-173.
23. G. Lazouzi, M. M. Vuksanović, N. Tomić, M. Mitrić, M. Petrović, V. Radojević, R. Jančić-Heinemann, Optimized preparation of alumina based fillers for tuning composite properties, Ceram. Int. 44 (2018) 7442-7449.
24. Z. Mojović, T. Novaković, M. Mojović, T. Barudžija, M. Mitrić, Electrochemical and Structural Properties of Ni(II)-alumina Composites as an Annealing Temperature Function, Sci. Sinter. 51 (2019) 339-351.
25. L. Dreval, T. Zienert, O. Fabrichnaya, Calculated phase diagrams and thermodynamic properties of the Al_2O_3-Fe_2O_3-FeO system, J. Alloys Compd. 657 (2016) 192-214.
26. A. Mahapatra, B. G. Mishra, G. Hota, Adsorptive removal of Congo red dye from wastewater by mixed iron oxide–alumina nanocomposites, Ceram. Int. 39 (2013) 5443-5451.
27. J. Wu, J. Wang, H. Li, Y. Du, K. Huang, B. Liu, Designed synthesis of hematite-based nanosorbents for dye removal, J. Mater. Chem. A. 1 (2013) 9837-9847.
28. S. Azizian, Kinetic models of sorption: a theoretical analysis, 276 (2004) 47-52.
29. Y. S. Ho, Review of second-order models for adsorption systems, 136 (2006) 681-689.
30. I. Chaari, B. Moussi, F. Jamoussi, Interactions of the dye, C.I. direct orange 34 with natural clay, J. Alloys Compd. 647 (2015) 720-727.
31. M. T. Yagub, T. K. Sen, S. Afroze, H. M. Ang, Dye and its removal from aqueous solution by adsorption: A review, Adv. Colloid Interface Sci. 209 (2014) 172-184.
32. Y. Bulut, H. Aydin, A kinetics and thermodynamics study of methylene blue adsorption on wheat shells, Desalination. 194 (2006) 259-267.
33. S. Banerjee, S. Dubey, R. K. Gautam, M. C. Chattopadhyaya, Y. C. Sharma, Adsorption characteristics of alumina nanoparticles for the removal of hazardous dye, Orange G from aqueous solutions, Arab. J. Chem. 12 (2019) 5339-5354.
34. P. Monash, G. Pugazhenthi, Utilization of Calcined Ni-Al Layered Double Hydroxide (LDH) as an Adsorbent for Removal of Methyl Orange Dye from Aqueous Solution, Environ. Prog. Sustain. Energy. 33 (2014) 154-159.
35. Z. Li, P. H. Chang, W. T. Jiang, J. S. Jean, H. Hong, Mechanism of methylene blue removal from water by swelling clays, Chem. Eng. J. 168 (2011) 1193-1200.
36. S. A. Singh, B. Vemparala, G. Madras, Adsorption kinetics of dyes and their mixtures with Co_3O_4-ZrO_2 composites, J. Environ. Chem. Eng. 3 (2015) 2684-2696.
37. J. Zolgharnein, M. Bagtash, T. Shariatmanesh, Simultaneous removal of binary mixture of Brilliant Green and Crystal Violet using derivative spectrophotometric determination, multivariate optimization and adsorption characterization of dyes on surfactant modified nano-γ-alumina, Spectrochim. Acta A Mol. Biomol. Spectrosc. 137 (2015) 1016-1028.
38. J. He, S. Hong, L. Zhang, F. Gan, Y. S. Ho, Equilibrium and thermodynamic parameters of adsorption of methylene blue onto rectorite, Fresenius Environ. Bull.

19 (2010) 2651-2656.
39. Y. H. Magdy, A. A. M. Daifullah, Adsorption of a basic dye from aqueous solutions onto sugar-industry-mud in two modes of operations, Waste Manag. 18 (1998) 219-226.
40. N. D. Hutson, R. T. Yang, Theoretical Basis for the Dubinin-Radushkevitch (D-R) Adsorption Isotherm Equation, Adsorption. 3 (1997) 189-195.
41. E. H. Mekatel, S. Amokrane, A. Aid, D. Nibou, M. Trari, Adsorption of methyl orange on nanoparticles of a synthetic zeolite NaA/CuO, Comptes Rendus Chim. 18 (2015) 336-344.
42. R. K. Gautam, P. K. Gautam, S. Banerjee, S. Soni, S. K. Singh, M. C. Chattopadhyaya, Removal of Ni(II) by magnetic nanoparticles, J. Mol. Liq. 204 (2015) 60-69.
43. R. I. Yousef, B. El-Eswed, A. H. Al-Muhtaseb, Adsorption characteristics of natural zeolites as solid adsorbents for phenol removal from aqueous solutions: Kinetics, mechanism, and thermodynamics studies, Chem. Eng. J. 171 (2011) 1143-1149.
44. G. Crini, P. M. Badot, Application of chitosan, a natural aminopolysaccharide, for dye removal from aqueous solutions by adsorption processes using batch studies: A review of recent literature, 33 (2008) 399-447.
45. A. Sari, M. Soylak, Equilibrium and thermodynamic studies of stearic acid adsorption on Celtek clay, J. Serb. Chem. Soc. 72 (2007) 485-494.

Сажетак: *Испитивана је адсорпција антрахинонске боје Кисело Плаве 111 (Acid Blue 111) честицама алуминијум (III) оксид-гвожђе допираних гвожђе оксидом припремљених сол-гел методом из водених раствора. Морфологија адсорбента испитивана је скенирајућом електронском микроскопијом (FESEM) а кристалографска фаза техником дифракције рендгенског зрака (XRD). Испитиван је утицај концентрације адсорбента и адсорбата, pX вредност и термодинамички параметри уклањања боје адсорпцијом. Промена концентрације боје током адсорпције праћена је коришћењем ултраљубичасте-видљиве (UV-Visible) спектрофотометрије. Површина адсорбента пре и након адсорпције боје посматрана је употребом инфрацрвене спектроскопије са Фуријеовом (Fourier) трансформацијом. Кинетика адсорпције показује најбоље поклапање са кинетичким моделом псеудо-другог реда. Ленгмирова (Langmuir) и Фројндлихова (Freundlich) адсорпциона изотерма су употребљене за описивање адсорпционог процеса. Термодинамичка студија адсорпције боје доказује да је процес спонтан са егсотермном природом.*

Кључне речи*: Отпадне воде текстилне индустрије; честице алуминијум (III) оксид допираних гвожђе оксидом; уклањање боје; карактеризација адсорбента; кинетичка студија.*

Supplementary material

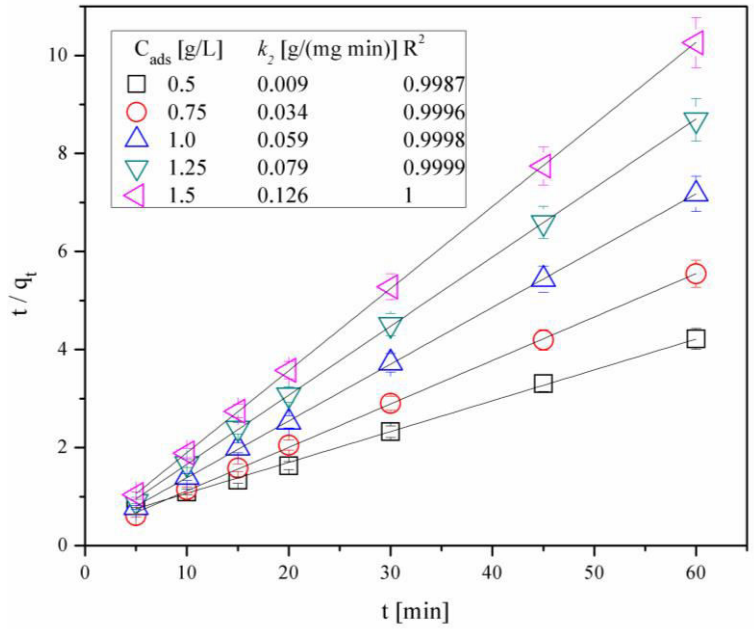

Fig. S1. Second-order kinetics plot for and the rate constants for AB111 dye removal at different initial alumina concentrations. Conditions: C_{AB111}= 100 mg/L, pH 3, T= 293.15 K, ω= 750 rpm.

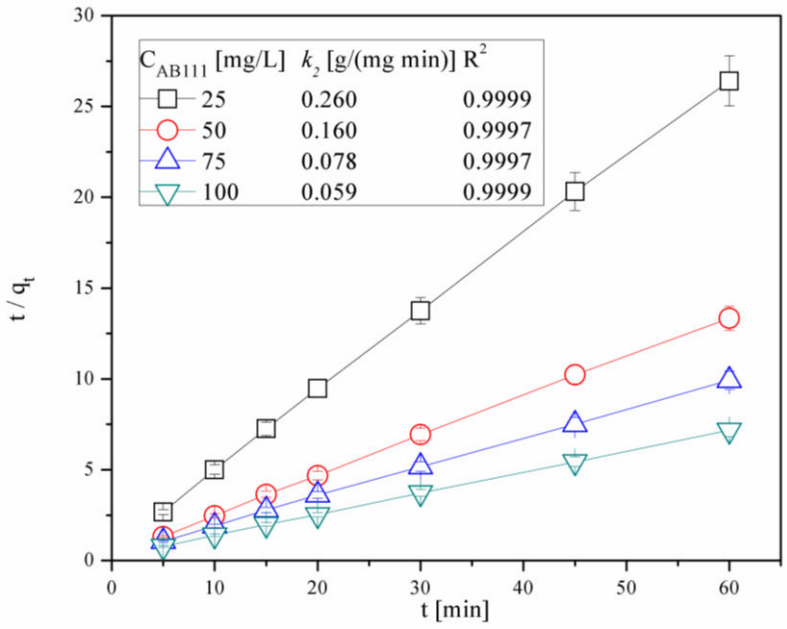

Fig. S2. Second-order kinetics plot for and the rate constants for AB111 dye removal at different initial dye concentrations. Conditions: C_{ads}=1 g/L, pH 3, T = 293.15 K, ω = 750 rpm.

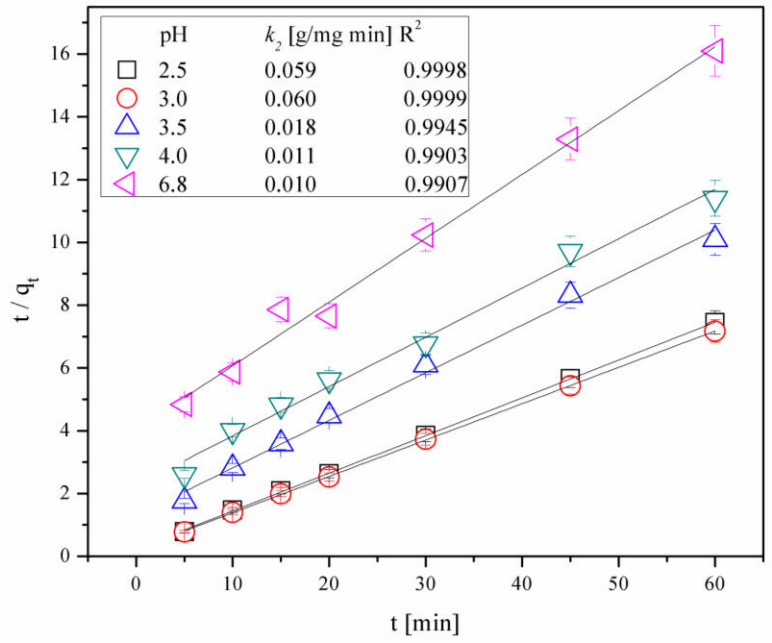

Fig. S3. Second-order kinetics plot for and the rate constants for AB111 dye removal at different initial pH values. Conditions: C_{AB111}=100 mg/L C_{ads}=1 g/L, T = 293.15 K, ω = 750 rpm.

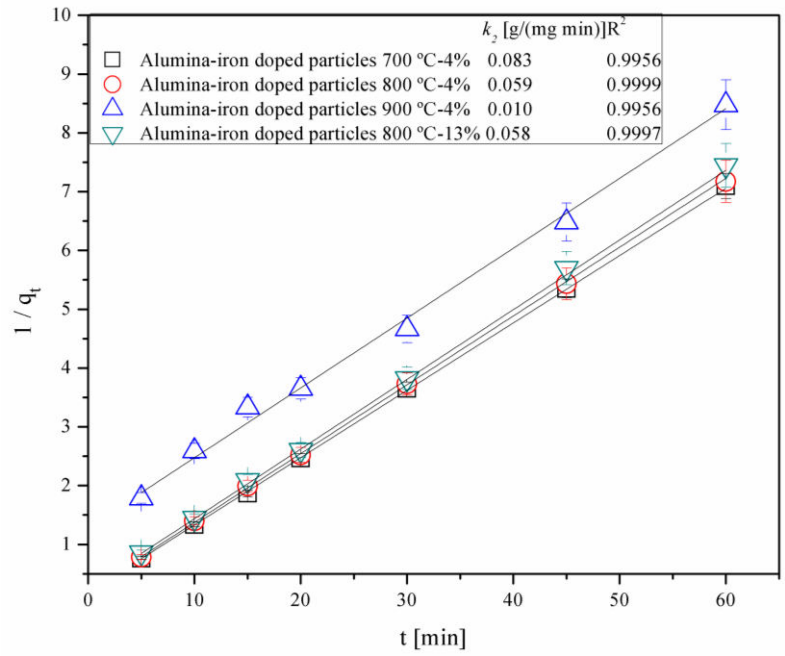

Fig. S4. Second-order kinetics plot for and the rate constants for AB111 dye removal at different initial pH values. Conditions: C_{AB111}=100 mg/L C_{ads}=1 g/L, pH 3, T = 293.15 K, ω = 750 rpm.

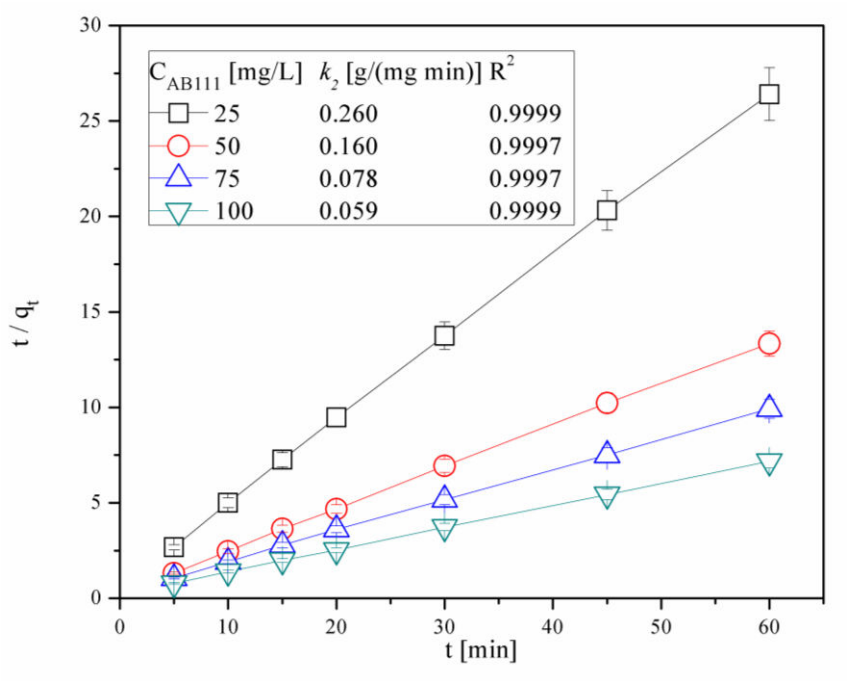

Fig. S5. Pseudo-second-order kinetics plot for and the rate constants for AB111 dye removal at different initial dye concentrations. Conditions: C_{ads}=1 g/L, pH 3, T = 293.15 K, ω = 750 rpm.

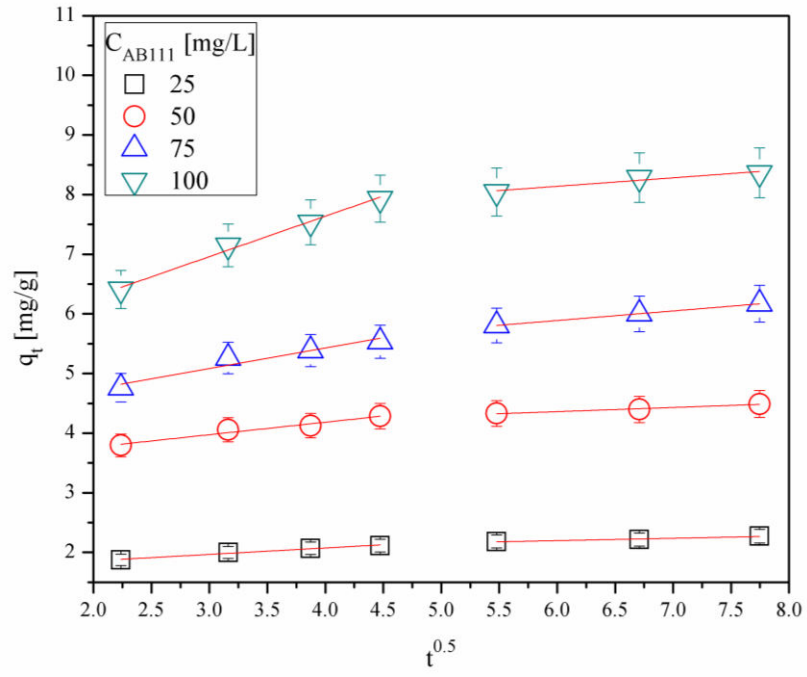

Fig. S6. Intra-particle diffusion plot for and the rate constants for AB111 dye removal at different initial dye concentrations. Conditions: C_{ads}=1 g/L, pH 3, T = 293.15 K, ω = 750 rpm.

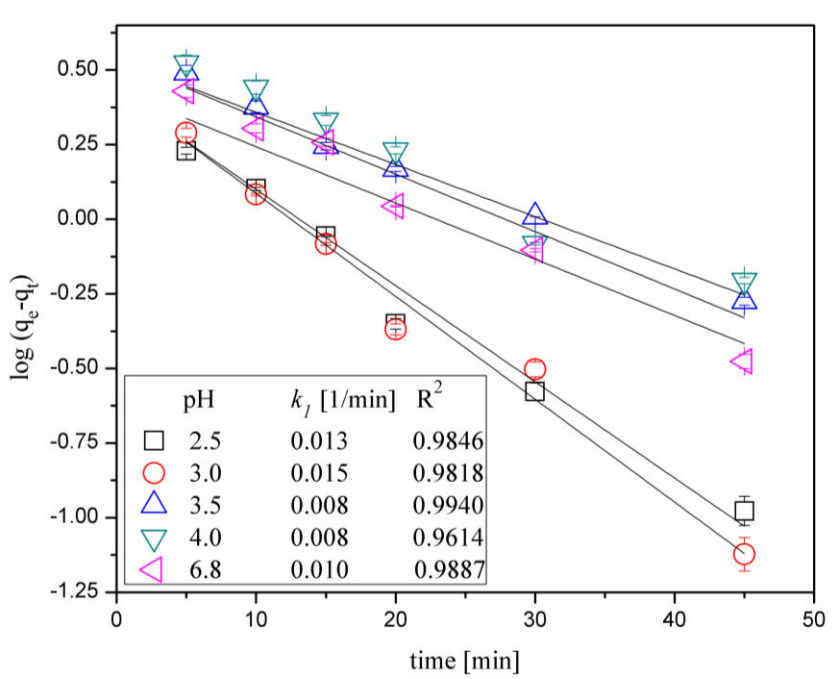

Fig. S7. Pseudo-first-order kinetics plot for and the rate constants for AB111 dye removal at different initial pH values. Conditions: C_{AB111}=100 mg/L C_{ads}=1 g/L, T = 293.15 K, ω = 750 rpm

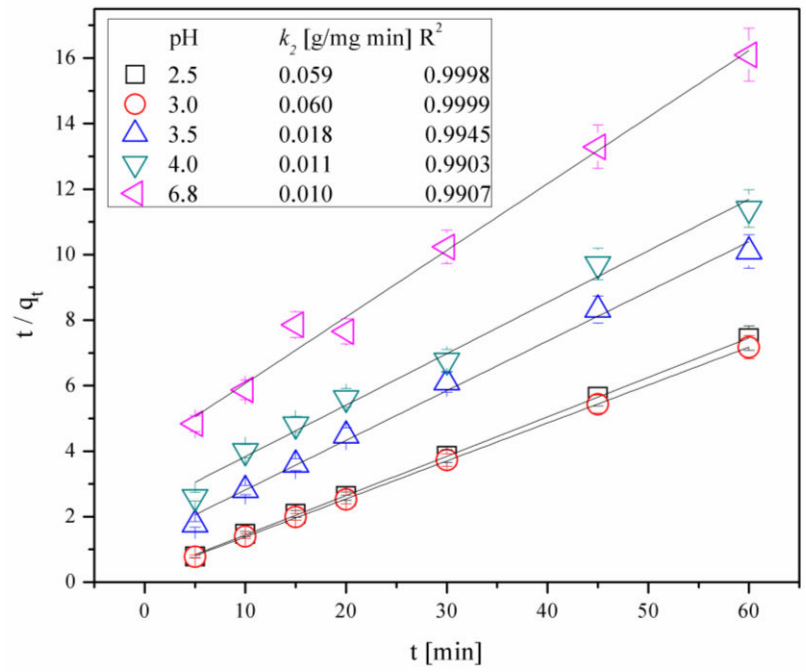

Fig. S8. Pseudo-second-order kinetics plot for and the rate constants for AB111 dye removal at different initial pH values. Conditions: C_{AB111}=100 mg/L C_{ads}=1 g/L, T = 293.15 K, ω = 750 rpm.

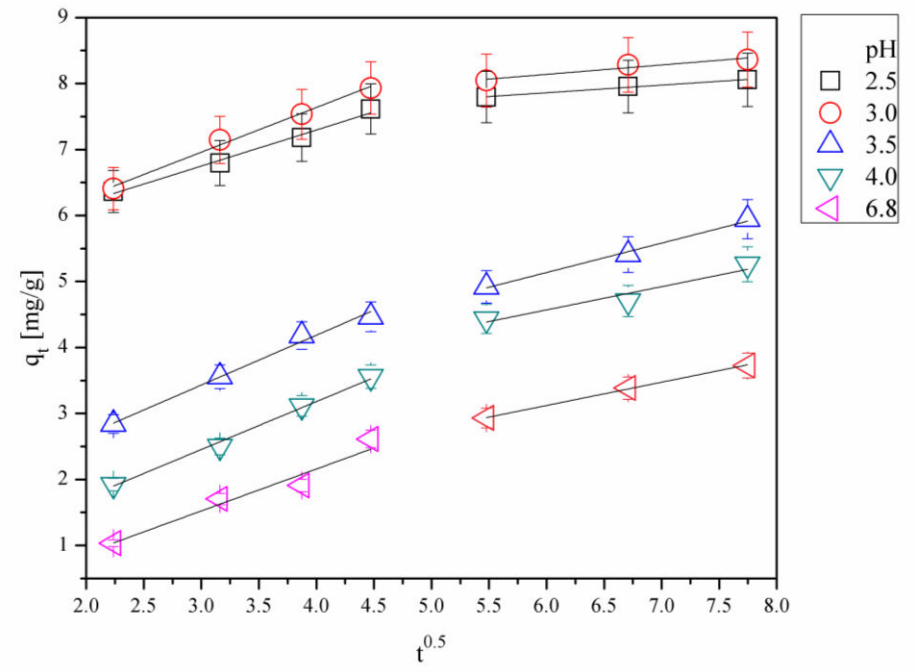

Fig. S9. Intra-particle diffusion plot for and the rate constants for AB111 dye removal at different initial pH values. Conditions: C_{AB111}=100 mg/L C_{ads}=1 g/L, T = 293.15 K, ω = 750 rpm.

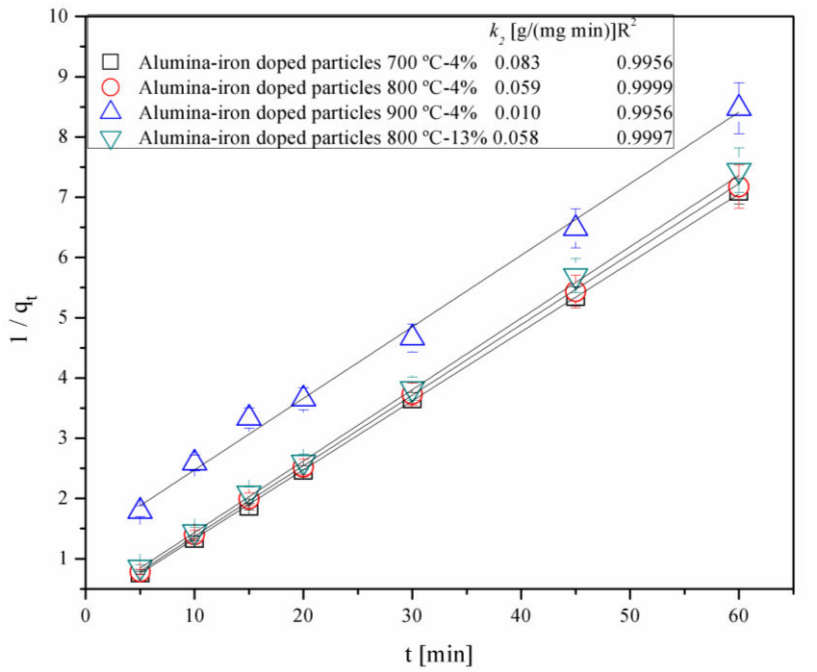

Fig. S10. Pseudo-second-order kinetics plot for and the rate constants for AB111 dye removal at different initial pH values. Conditions: C_{AB111}=100 mg/L C_{ads}=1 g/L, pH 3, T = 293.15 K, ω = 750 rpm